LERMA Observatoire de Paris | PSL

Explaining Spectral Line Profiles in the Horsehead Nebula Using Cloud Surface Curvature

Student
Ducheng Lu

Supervisors
Franck Le Petit (LERMA)
Emeric Bron (LERMA)

Jan 2025

Contents

Abstract

Context.
Aim.
Methods.
Results.

Abstract

Contexte.
Objectif.
Méthodes.
Résultats.

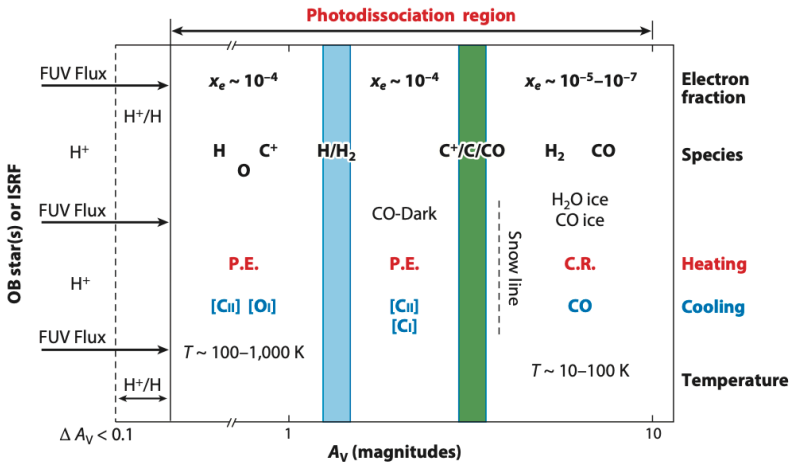

Figure 1: Schematic of a photodissociation region as a function of visual extinction A_V. Reprinted from Wolfire et al. (2022).

1 Introduction

The interstellar medium (ISM) is composed of gas and dust between stars in galaxies. The ISM is site of star formation and takes up around $\sim 10\%$ of total baryonic mass cite Drain2011. In return, the radiation field produced by stars is responsible for the heating the gas and dust that cool in bright line and continuum emission. These emission lines provide information about the physical conditions inside the ISM, such as the temperature, density and chemical composition.

Models have long been developed to help us interpret these

The 1D slab geometry may not be approprioate in some cases, and the curvature of the cloud surface needs to be taken into account in order to reproduce the line profiles. A common technique is to use a time-dependent hydrodynamic simulation to obtain the density and velocity fields and then to postprocess it with a PDR code to obtain the steady-state chemical abundances and thermal equilibrium gas temperature (e.g., Levrier et al. 2012).

1.1 Photodissociation Regions (PDRs)

Photodissociation regions (PDRs) are regions where far-ultraviolet (FUV; $6\,\mathrm{eV} < h\nu < 13.6\,\mathrm{eV}$) radiation dominates the chemistry or heating processes. cite Tielens & Hollenbach 1985a, Introduction in the annual review PDRs span a wide range of incident FUV fluxes and densities, including all neutral gas in the interstellar medium (ISM) and molecular layers where FUV radiation drives molecule formation.

1.2 The Horsehead Nebula

In order to compare with observations, we need to convert the distance unit cm used the in `MeudonPDR` code into the arcsec unit used in observation,

$$\alpha[''] = \frac{d\,[\mathrm{pc}]}{400\,\mathrm{pc}} \frac{1\,\mathrm{arcsec}}{1\,\mathrm{rad}} \tag{1}$$

where $400\,\mathrm{pc}$ (Menten et al. 2007; Schlafly et al. 2014) is the distance to the horsehead nebula.

Figure 2: Horsehead Nebula captured by the Hubble Space Telescope (HST) in 2013. The image was created from Hubble data from proposal 12812. Illustration Credit: NASA, ESA, and Z. Levay (STScI)

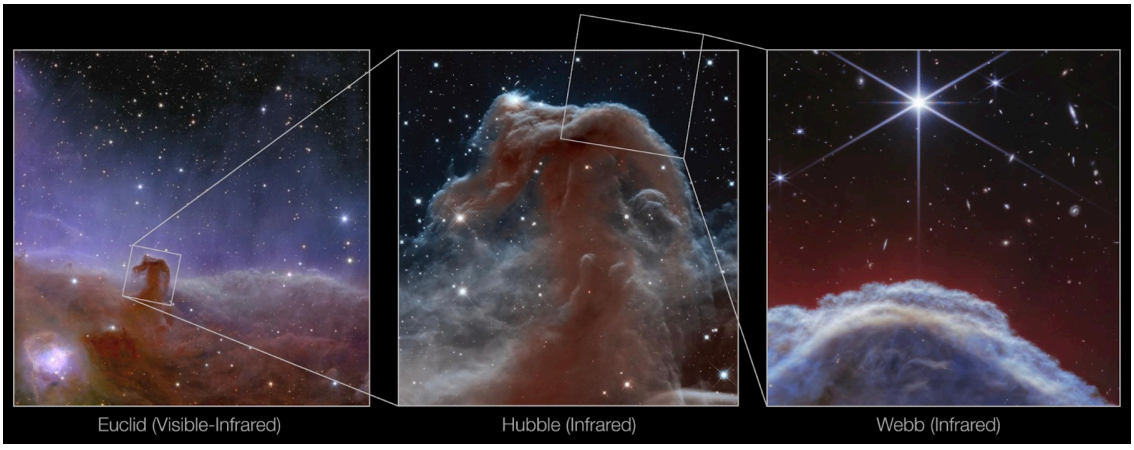

Figure 3: Three views of the Horsehead Nebula. The first image (left) features the Horsehead Nebula as seen by ESA's Euclid telescope. The second image (middle) shows the NASA/ESA Hubble Space Telescope's infrared view of the Horsehead Nebula. The third image (right) features a new view of the Horsehead Nebula from the NASA/ESA/CSA James Webb Space Telescope's NIRCam (Near-InfraRed Camera) instrument.

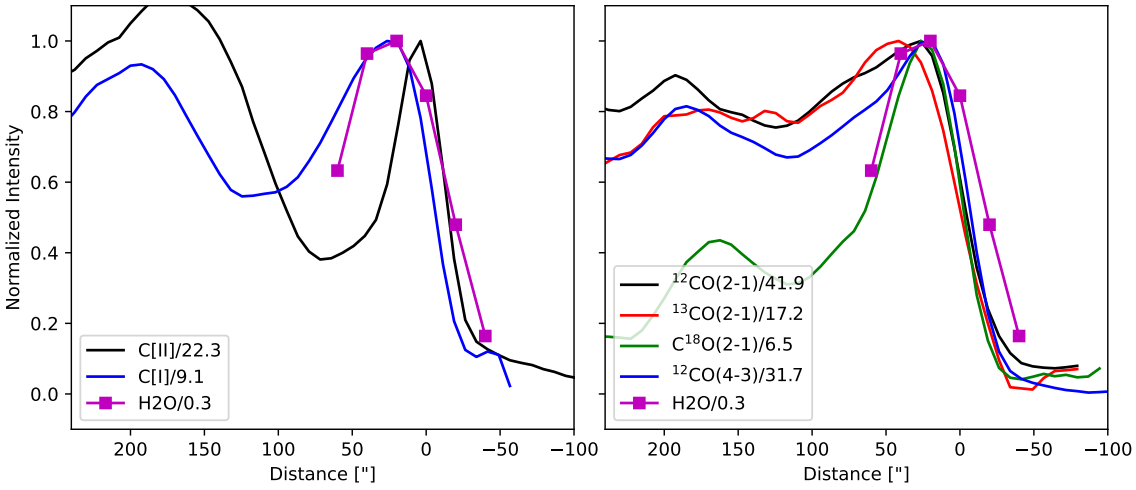

Figure 4: Observed line profiles of the Horsehead Nebula. Reproduced from cite the original paper. The ^{13}CO lines has been removed due to bad weather condition during the observation.

2 Data

In this report, my goal is to compare the observations of the Horsehead Nebula with the predictions of the `MeudonPDR` code. The observations were taken with Herschel. The data were taken from the original paper add citation.

3 Methods

3.1 The `MeudonPDR` code

A significant heterogeneity exists among the available PDR models, which differ in their geometry, physical and chemical structures, and model parameters. Röllig et al. (2007) suggest that the choice of a spedific code should depend on the physical and chemical processes implemented in the code, as well as the characteristics of the emission source.

In this project, I used the `MeudonPDR` code (Le Petit et al. 2006; Goicoechea and Le Bourlot 2007; Gonzalez Garcia et al. 2008; Le Bourlot et al. 2012; Bron 2014; Bron et al. 2014, 2016) to simulate the Horsehead Nebula. The `MeudonPDR` code models a stationary one-dimensional (1D), plane-parallel slab of gas and dust illuminated by an ultraviolet(UV) radiation field from one or both sides. At each iteration, the code solves the UV radiative transfer in both the continuum and lines, followed by the chemical balance, and finally the level populations and thermal balance.

3.1.1 Constant Pressure vs. Constant Density

The density structure of the PDR model, such as constant density, constant pressure, or a density profile specified by the user, can have a significant influence on the simulation results. Observations reveal that there is a steep density gradient in the PDRs of the Horsehead Nebula (Habart et al. 2005; Guzmán et al. 2011) in C. Hernández-Vera 2023. Hernández-Vera 2023 verified that the observations cannot be reproduced by a constant density model, yet neither by previously proposed density profile prescriptions. Later, observations by ALMA and Herschel suggest that the warm layer of PDRs is indeed isobaric with relatively large thermal pressures (Marconi et al. 1998; Goicoechea et al.

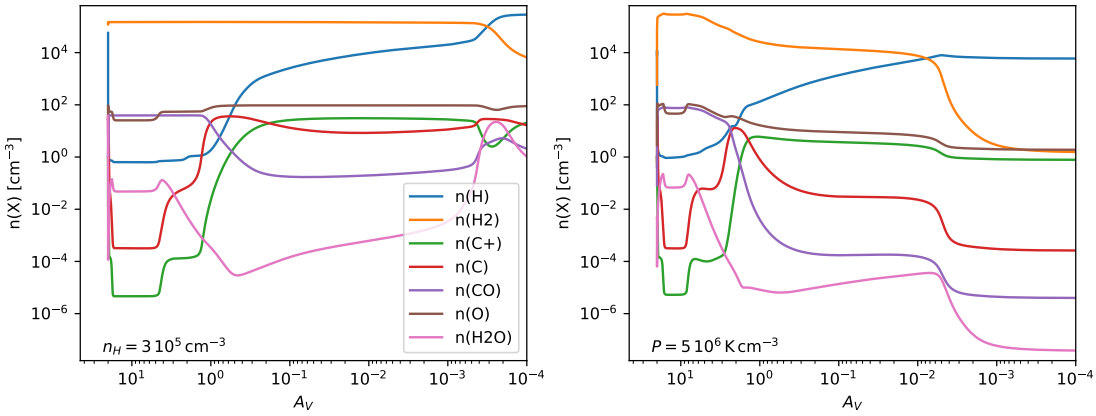

Figure 5: Comparison of the cloud structure computed with constant density (left) and constant pressure (right).

2016; Joblin et al. 2018; Wu et al. 2018; Bron et al. 2018; Maillard et al. 2021). For this reason, we use the constant pressure model in the `MeudonPDR` code.

The density structure of a photodissociation region model—whether constant density, constant pressure, or a user-defined density profile—can significantly influence the simulation results cite annual review. Observations of the Horsehead Nebula reveal a steep density gradient in the PDRs Habart 2005, Guzmán 2011, Hernández-Vera 2023. Hernández-Vera (2023) showed that constant density models cannot reproduce observations, nor by previously proposed density profile prescriptions. Furthermore, recent observations from ALMA and Herschel indicate that the warm layer of PDRs is indeed isobaric, characterized by relatively high thermal pressures Marconi 1998, Goicoechea 2016, Joblin 2018, Wu 2018, Bron 2018, Maillard 2021. For this reason, I use the constant pressure model in the `MeudonPDR` code for my study.

As shown in Fig. 5, I compare the cloud structure computed with constant pressure and constant density assumptions, illustrating the differences in the resulting PDR structures.

3.1.2 Models with Radiative Transfer of H_2

3.1.3 Models with Surface Chemistry

3.2 Geometry

In order to model the curvature of the cloud surface, we approximate the surface using plane-parallel geometry, as shown in Fig. 6.

More precisely, we consider the PDR region as the outermost shell embedded in a fictitious spherical cloud, whose radius R will need to be determined by the user and is given as a parameter to the wrapper code.

A line of sight will be defined by an impact parameter b, which is the distance from the line-of-sight (LoS) to the center of the cloud.

From the output of the `MeudonPDR` code, we have the number densities of levels as a function of the depth into the cloud, so we need to know the depth (i.e., the distance to the cloud surface) corresponding to each point along the LoS, we denote this quantity as d.

Using Pythagorean theorem, we can easily establish that

$$d = R - \sqrt{s^2 + b^2} \tag{2}$$

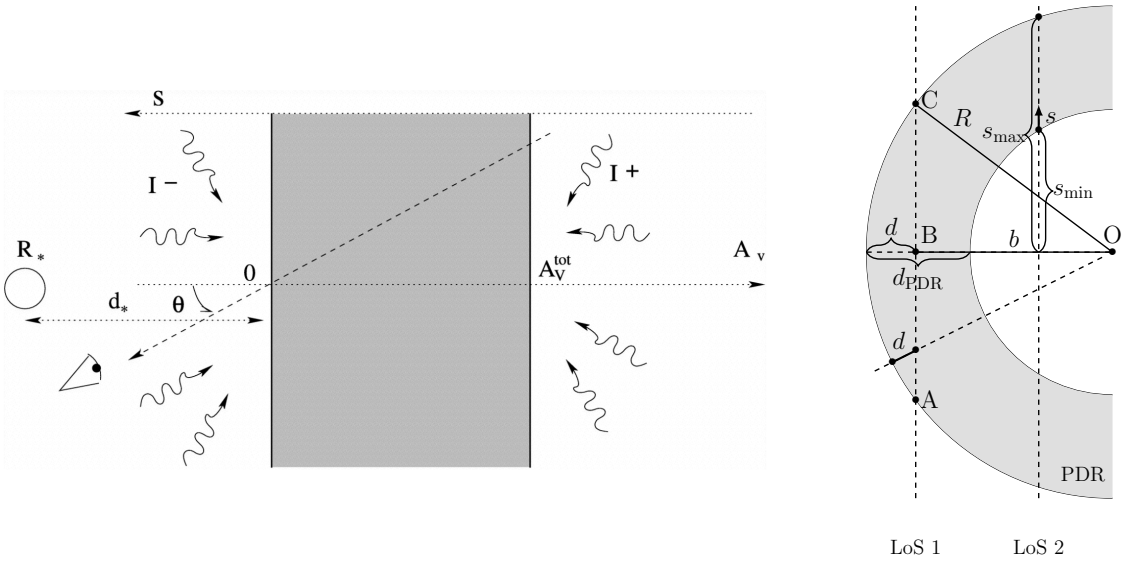

Figure 6: Left: scheme of the slab geometry of the `MeudonPDR` code. Reprinted from Le Petit et al. (2006) Right: scheme of the plane-parallel geometry of the PDR wrapper.

3.3 Column Density

The wrapper code take as input:

- the level number densities computed by the MeudonPDR code, as a function of the depth into the cloud, $n_X(d)$;
- the radius of the fictitious spherical cloud, R;
- the impact parameter of the LoS, b.

The algorithm goes as follow

1. interpolate the level number density to enable the computation of the density at any valid given value of depth, $n_X(d) = f(d)$;
2. compute the range of distances inside the PDR region along the LoS

$$s_{\text{max}} = \sqrt{R^2 - b^2}, s_{\text{min}} = \begin{cases} 0 & b > R - d_{\text{PDR}} \\ \sqrt{(R - d_{\text{PDR}})^2 - b^2} & b < R - d_{\text{PDR}} \end{cases} \quad (3)$$

3. convert the distance along the LoS to depth from the surface of the cloud, and compute the level number density

$$n_X(s) = f(R - \sqrt{s^2 + b^2}); \quad (4)$$

4. the column density for a given LoS with impact parameter b is given by

$$N_X(b) = 2 \int_{s_{\text{min}}}^{s_{\text{max}}} n_X(s') \mathrm{d}s'. \quad (5)$$

3.4 Radiative transfer equation

In the previous calculation of the column densities, we have made the assumption that all lines are optically thin; in fact, some of the lines can be optically thick, which explains the difference in the shape of the curve in observations for different lines in Fig 4.

To account for line extinction inside the cloud, we need to solve the radiative transfer equation along the LoS cite see, for example, Eq (1.67) Rybicki?:

$$\frac{\mathrm{d}I_\nu}{\mathrm{d}s} = A_{ul} n_u \frac{h\nu}{4\pi}\phi(\nu) + B_{ul} n_u \frac{h\nu}{4\pi} I_\nu \phi(\nu) - B_{lu} n_l \frac{h\nu}{4\pi} I_\nu \phi(\nu), \tag{6}$$

where n_u and n_l are the number densities of the upper and lower levels of the transition, respectively, h is the Planck's constant, ν is the frequency of the transition, and $\phi(\nu)$ is the line profile. We assume that the emission and absorption profiles are the same and we neglect scattering justify?. A_{ul}, B_{ul}, B_{lu} are the Einstein coefficients for this transition, which are related by the Einstein relation references

$$B_{ul} = \frac{c^2}{2h\nu_{ul}^3} A_{ul},\ g_l B_{lu} = g_u B_{ul}, \tag{7}$$

where g_u and g_l are the degeneracies of the upper and lower levels, respectively.

For consistency, we keep the same values for the Einstein coefficients as in the `MeudonPDR` code, which are taken from references?.

In the PDR, turbulences are the dominant line broadening process references? a bit more on line broadening in the intro?, in which case the line profile $\phi(\nu)$ is a Gaussian profile in the form references

$$\phi(\nu) = \frac{1}{\sigma_\nu \sqrt{2\pi}} \exp\left(-\frac{(\nu-\nu_0)^2}{2\sigma_\nu^2}\right), \tag{8}$$

where

$$\sigma_\nu = \frac{\sqrt{2}}{2}\Delta\nu_D,\ \Delta\nu_D = \frac{\nu_0}{c}\sqrt{\frac{2kT}{m} + v_{\mathrm{turb}}^2}. \tag{9}$$

The turbulent velocity v_{turb} is a parameter in the `MeudonPDR` code, with a default value of $2\,\mathrm{km\,s^{-1}}$. T is the temperature, and m is the mass of the line-emitting species. For the mass we use the same value as the `MeudonPDR` code (as defined in , taken from Scientific Instrument Services (SIS) database? change name?

The line profile is normalized so that $\int_0^\infty \phi(\nu)\mathrm{d}\nu = 1$. In practice, we truncate the line profile at 5σ add a figure to demonstrate that this is reasonable for the lines concerned?, i.e., the normalization becomes

$$\int_{\nu_0-5\sigma}^{\nu_0+5\sigma} \phi(\nu)\mathrm{d}\nu = 1 \tag{10}$$

To solve the radiative transfer equation, we also need a background intensity I_0. For this we use the isotropic specific intensity on the observation side output by the `MeudonPDR` code, in the `_IncRadField.dat` file. add explanation that our implementation is only valid for isotropic radiation and explains why we couldn't implement a more generic background specific intensity.

The external radiation field in the `_IncRadField.dat` file is in units of $\mathrm{erg\,cm^{-2}\,s^{-1}\,sr^{-1}\,Å^{-1}}$, so we need to convert the specific intensity in to $\mathrm{erg\,cm^{-2}\,s^{-1}\,sr^{-1}\,Hz^{-1}}$,

$$I_\nu|\mathrm{d}\nu| = I_\lambda|\mathrm{d}\lambda| \Rightarrow I_\nu = I_\lambda\left|\frac{\mathrm{d}\lambda}{\mathrm{d}\nu}\right| = I_\lambda\frac{c}{\nu^2} = I_\lambda\frac{\lambda^2}{c} \tag{11}$$

$$\lambda = \frac{c}{\nu} \Rightarrow \mathrm{d}\lambda = -\frac{c}{\nu^2}\mathrm{d}\nu \Rightarrow \left|\frac{\mathrm{d}\lambda}{\mathrm{d}\nu}\right| = \frac{c}{\nu^2} = \frac{\lambda^2}{c} \tag{12}$$

It is often more convenient to do a change of variable and integrate over optical depth

$$\frac{\mathrm{d}I_\nu}{\mathrm{d}\tau_\nu} = S_\nu - I_\nu, \tag{13}$$

with

$$\tau_\nu = \alpha_\nu \mathrm{d}s,\ S_\nu = \frac{j_\nu}{\alpha_\nu} \tag{14}$$

$$\alpha_\nu = \frac{h\nu}{4\pi}\phi(\nu)(B_{lu}n_l - B_{ul}n_u) \tag{15}$$

$$j_\nu = A_{ul}n_u\frac{h\nu}{4\pi}\phi(\nu) \tag{16}$$

To test the solver, we first solve the radiative transfer with constant density profiles of both the lower and upper level, then the radiative transfer equation becomes

$$\frac{\mathrm{d}I_\nu}{\mathrm{d}s} = c_1 + c_2 I_\nu, \tag{17}$$

with

$$c_1 = A_{ul}n_u\frac{h\nu}{4\pi}\phi(\nu) = \text{cst}$$
$$c_2 = (B_{ul}n_u - B_{lu}n_l)\frac{h\nu}{4\pi}\phi(\nu) = \text{cst}.c$$

The analytical solution is

$$I_\nu(s) = (I_0 + \frac{c_1}{c_2})e^{c_2 s} - \frac{c_1}{c_2}. \tag{18}$$

For example, if we consider the CO transition from v = 0, J = 2 to v = 0, J = 1, with a constant density profile of $n_u = 2\,\mathrm{cm}^{-3}$, $n_l = 2\,\mathrm{cm}^{-3}$, $A_{ul} = 6.911 \times 10^{-7} s^{-1}$

- $h\nu/4\pi = 4.86234284e-16$
- $A_{ul} = 6.911e-07$
- $B_{ul} = 3825410.21021763$
-

3.5 Convolution

4 Results and Discussion

4.1 Cloud Surface Curvature

4.2 Line Profiles

5 Conclusions

References

Le Petit, Franck et al. (2006). "A Model for Atomic and Molecular Interstellar Gas: The Meudon PDR Code". In: ApJS 164.2, pp. 506–529. DOI: 10.1086/503252.

Goicoechea, J. R. and J. Le Bourlot (2007). "The penetration of Far-UV radiation into molecular clouds". In: A&A 467.1, pp. 1–14. DOI: 10.1051/0004-6361:20066119.

Menten, K. M. et al. (2007). "The distance to the Orion Nebula". In: A&A 474.2, pp. 515–520. DOI: 10.1051/0004-6361:20078247.

Gonzalez Garcia, M. et al. (2008). "Radiative transfer revisited for emission lines in photon dominated regions". In: A&A 485.1, pp. 127–136. DOI: 10.1051/0004-6361:200809440.

Le Bourlot, J. et al. (2012). "Surface chemistry in the interstellar medium. I. H_2 formation by Langmuir-Hinshelwood and Eley-Rideal mechanisms". In: A&A 541, A76, A76. DOI: 10.1051/0004-6361/201118126.

Bron, Emeric (2014). "Stochastic processes in the interstellar medium". 2014PA077169. PhD thesis, 1 vol. (382 p.)

Bron, Emeric, Jacques Le Bourlot, and Franck Le Petit (2014). "Surface chemistry in the interstellar medium. II. H_2 formation on dust with random temperature fluctuations". In: A&A 569, A100, A100. DOI: 10.1051/0004-6361/201322101.

Schlafly, E. F. et al. (2014). "A Large Catalog of Accurate Distances to Molecular Clouds from PS1 Photometry". In: ApJ 786.1, 29, p. 29. DOI: 10.1088/0004-637X/786/1/29.

Bron, Emeric, Franck Le Petit, and Jacques Le Bourlot (2016). "Efficient ortho-para conversion of H_2 on interstellar grain surfaces". In: A&A 588, A27, A27. DOI: 10.1051/0004-6361/201527879.

Wolfire, Mark G., Livia Vallini, and Mélanie Chevance (2022). "Photodissociation and X-Ray-Dominated Regions". In: *Annual Review of Astronomy and Astrophysics* 60.Volume 60, 2022, pp. 247–318. DOI: https://doi.org/10.1146/annurev-astro-052920-010254.